JNCS Journal of Nepal Chemical Society July 2025, Vol. 45, No. 2, 11-24
ISSN: 2091-0304 (print)
DOI: https://doi.org/10.3126/jncs.v45i2.82919
RESEARCH ARTICLE

Exploring the Structural, Electronic, and Magnetic Properties of $MoTe_2$ and $MoSe_2$ Materials Via DFT+U Approach

Arpan Pokharel, Kamal Khanal, Sukrit Kumar Yadav, Tejendra Neupane, GaneshPaudel, Om Shree Rijal, and Hari Krishna Neupane*

Amrit Campus, Institute of Science and Technology, Tribhuvan University, Kathmandu Nepal.

**Corresponding Email: hari.neupane@ac.tu.edu.np*

Received: May 15, 2025, Revised: June 14, 2025, Accepted: 15 July, 2025)

Abstract

Two-dimensional (2D) transition metal dichalcogenides (TMDCs) materials have potential applications in the fields of electronic and optoelectronic devices. In the present work, we have studied the structural, electronic, magnetic, and dynamical properties of $MoSe_2$ and $MoTe_2$ (3×3) supercell monolayer structures using the density functional theory (DFT) method with the PBE+U functional, employing the quantum ESPRESSO computational package. The structural properties of the considered materials are studied by the analysis their estimated ground state energy and bond length between nearest-neighbors atoms present in the structures. $MoSe_2$ and $MoTe_2$ materials are found to be structurally stable, having hexagonal structures. To predict the electronic and magnetic properties of the materials, we have interpreted their band structure, density of states (DoS), and partial density of states (PDoS) plots. From the discussion, it is found that $MoTe_2$ and $MoSe_2$ have small band gap and non-magnetic properties. Hence, they are classified as small band gap semiconducting, non-magnetic materials. Moreover, we have developed the phonon dispersion curves to predict dynamical stability of the materials. It is found that all the frequencies at each symmetric points of the considered materials have positive values. This implies that they are dynamically stable materials. Hence, based on the analysis of the electronic, magnetic and dynamical properties of $MoTe_2$ and $MoSe_2$ materials, they can be used in the fields of electronic and optoelectronic device applications.

Keywords: DFT, Electronic, Magnetic, Monolayer, Phonon, Semiconductor.

Introduction

The discovery of transition metal dichalcogenides (TMDCs) materials has been transformative for modern science. The emergence of TMDCs materials is due to the attributed to the availability of various structural forms such as monolayers, multilayers, heterostructures, and bulk structures. Mostly, monolayers are used in the field effect transistor (FET), photodetectors, flexible and transparent electronics, sensors; multilayers are used in memory devices, thermoelectric devices, photovoltaics; heterostructures are used in the spintronics and optoelectronics devices; and bulk structures are used in the thermal coatings, and catalysis etc. Thus, these materials are good candidates for real-world applications [1-5]. TMDCs materials have form the formula TC_2 (such as $MoTe_2$, $MoSe_2$, WSe_2, etc.), where T is a transition metal like Mo or W etc. and C represents chalcogens like Te_2 or Se_2 etc. [1, 4]. Mo-based TMDCs materials have been garnering attention in recent times due to their unique and wide range (1.50 eV to 3.90 eV) of properties [6-8]. They mostly exhibit semiconducting behavior with a wide range of

band gap energies. In some cases, band gap energy depends on the number of layers in the material. However, it can be modified by doping or creating vacancy defects as needed, which opens door for the development of better microprocessors and other electronic devices [9-11]. The Mo-based TMDCs have one Mo atom lodged between two chalcogen atoms [1, 6]. Both of these materials primarily crystallize in either of hexagonal or monoclinic phase, depending on the temperature of formation [7, 8]. Additionally, TMDCs materials exhibit different magnetic properties depending on their phase and purity. These properties can be altered with the help of vacancy or doping [12-14]. Therefore, they are also well suited for spintronics applications; that is, they can be used in nanotechnology, biomedicine, cloaking, energy harvest, and other fields [15, 16].

Numerous studies on Mo-based TMDCs materials have been reviewed, and various parameters, such as band gap energy and the distribution of spin states in atomic orbitals etc., have been calculated using density functional theory (DFT) technique with the GGA: PBE functional [1, 6, 9, 12]. To our best knowledge, no thorough computational analysis of Mo-based $MoTe_2$ and $MoSe_2$ TMDCs materials using the PBE+U functional has been reported in the literature. Thus, we are prompted to investigate the structural, dynamical, electronic, and magnetic properties of $MoTe_2$ and $MoSe_2$ TMDCs materials based on the DFT approach using the PBE+U functional, employing the computational tool Quantum ESPRESSO. Multiple physical properties of TMDCs materials using the DFT method based on the PBE functional have been are reported [17-19]. However, the PBE+U functional uses the Hubbard potential (U) with the GGA: PBE functional, which significantly affects the physical properties of materials. Moreover, we have not found any reported studies investigation the electronic, magnetic, and dynamical properties of $MoTe_2$ and $MoSe_2$ compounds using the DFT method with the PBE+U functional because for elements with d-orbitals in the structure, the inclusion of the U parameter is more suitable for accurately estimating their band gap energy. This represents the research gap between previously reported works and present study. Hence, we explored the structural, electronic, magnetic, and dynamical properties of $MoTe_2$ and $MoSe_2$ (3×3) supercell monolayer TMDCs materials using the DFT method with the PBE+U functional.

Materials and Methods

This work was conducted within the quantum mechanical framework by employing the density functional theory (DFT) method. All DFT calculations were performed using a plane wave basis set with the computational tool Quantum ESPRESSO (QE) [20-23]. The PBE+U functional was utilized alongside the generalized gradient approximation (GGA) approach with ultrasoft pseudopotentials (USPS) to calculate the exchange-correlation energy (E_{Xc}) [24-26]. In the present work, the electron correlation energy was determined using the PBE+U functional, where U denotes the Hubbard potential (i.e., U_p = 3 eV was used to p-orbitals, and U_d = 5 was used to d-orbitals of atoms in the structures) [21, 23]. Additionally, the software packages XCrySDen and Xmgrace were used for crystal structure visualization and graph plotting, respectively [27]. First, the unit cell structures of the considered materials were optimized using self-consistent fields (scf) calculations, in which k-points, kinetic energy cutoff, and lattice parameters were estimated. The kinetic energy cutoff values for $MoTe_2$ and $MoSe_2$ materials were found to be 690 eV (50.71 Rydberg) and

471 eV (34.61 Rydberg), respectively. These estimated parameters were used in the input file, after which relax calculation were performed. The relaxed structures of $MoTe_2$ and $MoSe_2$ were obtained. Subsequently, the optimized and relaxed (3×3) supercell structures of $MoTe_2$ and $MoSe_2$ materials were created, as shown in **Figure 1.** These supercell structures were prepared by extending the unit cell structures three times along the x-axis and three times along the y-axis. The supercell structures were then again relaxed for further calculations. The reciprocal lattice was sampled by using an (8×8×1) Monkhorst-Pack (MK) k-point grid [28]. The Gamma-centered k-point grid was used due to its low computation cost. Moreover, density of states (DoS) and partial density of states (PDoS) calculations were performed on a denser (24×24×1) grid for more resolved and smooth plots. After that, we estimated the ground state energy of the materials and the bond lengths of atoms present in the structures to determine the structural properties. Electronic and magnetic properties were studied using band-DoS and DoS-PDoS plots. Finally, the dynamical stability of $MoTe_2$ and $MoSe_2$ materials was predicted using phonon dispersion curves for the PBE+U functional.

Results and Discussion

In this section, we discuss the structural, electronic, magnetic, and dynamical properties of the (3×3) supercell structures of $MoTe_2$ and $MoSe_2$ materials using the DFT approach. Additionally, we compare our findings with the available data from reported studies on similar materials.

Structural Properties

The structural properties of $MoTe_2$ and $MoSe_2$ materials are studied using their estimated ground state energy, and the bond length between the nearest atoms in the materials. The lattice constant (a) values for $MoTe_2$ and $MoSe_2$ are found to be 5.90 Å and 5.83 Å, respectively. The optimized and relaxed structures of $MoTe_2$ and $MoSe_2$ TMDCs materials are shown in figures-1(a, b) and 1(c, d), respectively.

The structures of $MoTe_2$ and $MoSe_2$ are hexagonal when observed from the front side; however, the atoms in the structures are arranged in a zigzag pattern when viewed from the top side. The difference between structures before and after relaxation can be seen by comparing the interatomic distances between atoms. We measured the interatomic distances between Mo-Se, Mo-Te, Te-Te, and Se-Se atoms in both structures and found them to be equal. The interatomic distance between Mo-Se and Mo-Te atoms before relaxation is found to be 2.53 Å, whereas Mo-Mo, Se-Se, and Te-Te atoms in the structures have an equal separation of 3.32 Å. Similarly, after relaxation, the bond length changes to 2.54 Å for Mo-Se and Mo-Te atoms, which is in good agreement with the previously reported value of 2.73 Å for TMDCs materials [7]. The interatomic distances of Mo-Mo, Se-Se, and Te-Te atoms are measured to be 3.31 Å, indicating a decrease to 3.31 Å, which is also close to the previously reported value of 3.51 Å [29]. From these calculations, it is found that the interatomic distance between molybdenum and chalcogen atoms increases after relaxation. Hence, similar atoms (i.e., Mo-Mo, Te-Te & Se-Se) become more compact after relaxation. This discrepancy in the interatomic distances can be attributed to the random configuration and excited energy of atoms before relaxation. After relaxation, however, all the forces cancel out, and the system attains minimum energy because relaxation process minimizes the total energy of the system by adjusting atomic coordinates and possibly the cell dimensions. This process obeys the principle of minimum energy, which states that stable structures exist at local or global minima of the potential energy surface.

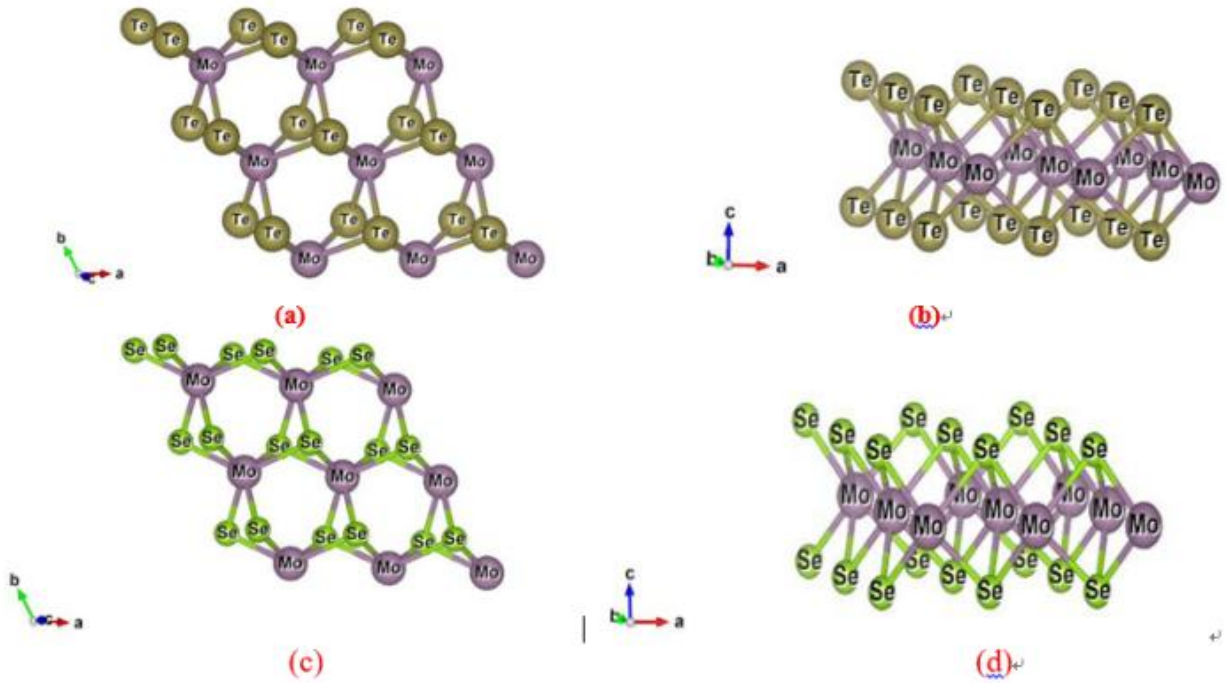

Figure 1: (Color online) (a) Front view of (3×3) supercell $MoTe_2$ after relaxation, (b) Top view of (3×3) supercell $MoTe_2$ after relaxation, (c) Front view of (3×3) supercell $MoSe_2$ after relaxation, and (d) Top view of (3×3) supercell $MoSe_2$ after relaxation.]

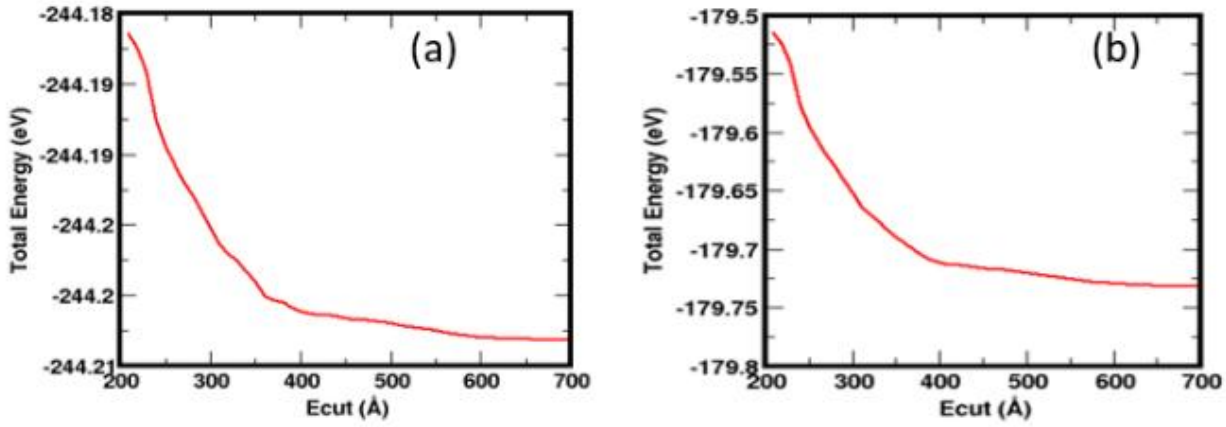

Figure 2: (Color online) (a) Optimization vs changes in energy of $MoTe_2$ and of $MoSe_2$ materials before relax calculations, and (b) Optimization vs changes in energy of $MoTe_2$ and of $MoSe_2$ materials after relax calculations.]

Table 1: The interatomic distances between atoms present in MoX_2 materials where, E & R represent estimated and reported values respectively, X represents Te & Se atoms, and E_g represents the ground state energy of materials.

State	Mo-X (X=Te, Se) (E)	Mo-X (R)	Mo-Mo (E)	Mo-Mo (R)	X-X (E)	X-X (R)	E_g of $MoTe_2$	E_g of $MoSe_2$
Before Relaxation	2.53 Å	-	3.32 Å	-	3.32 Å	-	-179.71 (eV)	-179.71 (eV)
After Relaxation	2.54 Å	2.73 Å [7]	3.31 Å	3.51 Å [25]	3.31 Å	3.51 Å [29]	-244.20 (eV)	-244.20 (eV)

We obtained the energy optimization plots before and after the relaxation calculations, which are illustrated in **Figure 2(a) and 2(b)**, respectively. It is observed that the ground state energy of the relaxed 2D monolayer $MoTe_2$ and $MoSe_2$ is equal to -244.20 eV. This value is lower than the energy values obtained for $MoTe_2$ and $MoSe_2$ before the relaxation calculations. Hence, the materials are structurally stable, as materials with lower ground state energy and higher binding energy are generally more stable. The estimated values of ground states energy and interatomic distances for $MoSe_2$ and $MoTe_2$ materials are given in Table-1.

Electronic properties

We have studied the electronic properties of monolayer $MoTe_2$ and $MoSe_2$ materials using band structure and density of states (DoS) plots.

Band Structure

We have analyzed band structures of $MoTe_2$ and $MoSe_2$ materials to study their electronic properties, which are illustrated in figures-3(a) and 3(b). In both structures, the horizontal dotted line represents the Fermi energy level, and the vertical dotted lines denote high-symmetric points. Here, Γ represents the center of irreducible Brillouin zone (BZ).

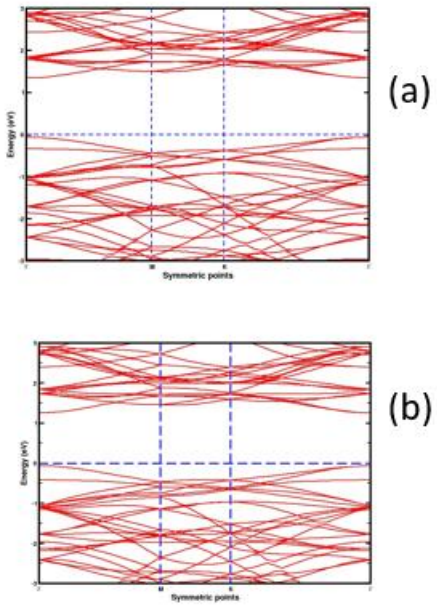

Figure 3: (Color online) (a) band structure of $MoTe_2$, and (b) band structure of $MoSe_2$, where Fermi level is set at 0 eV. The horizontal dotted line represents Fermi level and vertical dotted line represents high symmetric points.]

These symmetry points have been used to determine whether the material has a direct or indirect band gap. From the analysis of materials band structures, it is found that the Fermi level is close to the valence region, and both the conduction band minimum (CBM) and valence band maximum (VBM) lie at high-symmetric point Γ, indicated that they have direct band gap semiconducting properties.

This means, $MoTe_2$ and $MoSe_2$ have electron momentum that does not change during transition. Moreover, a greater number of band states are presented in the valence band region compared to the conduction band region.

Table 2: Fermi energy (E_f), conduction band minimum (E_{CBM}), valence band maximum (E_{VBM}), and band gap energy (E_g) of monolayer $MoTe_2$ and $MoSe_2$ supercell structures.

Parameter	$MoTe_2$ (eV)	$MoSe_2$ (eV)
E_f	-0.70	-0.54
E_{CBM}	0.63	0.70
E_{VBM}	-0.77	-0.61
E_g	1.40	1.31

Additionally, no band crosses from the conduction region into the valence region or vice versa, which further supports that our materials are non-metallic in nature. The energies difference between the CBM and VBM of $MoTe_2$ gives its band gap, which is found to be 1.40 eV, which is comparatively close to other computationally calculated values of 1.23 eV, 1.23 eV and 1.18 eV for TMDCs materials [10, 11, 13, 30]. These estimated values of band gap energies are slightly greater than the experimental reported value of 1.10 eV for TMDCs materials [10]. Also, the band gap energy of $MoSe_2$ is found to be 1.31 eV, which is in good agreement with the computationally reported value of 1.44 eV [10, 11, 30, 31], and the experimental reported value of 1.50 eV for others materials [10, 32]. From these calculations, it is found that $MoSe_2$ has a slightly smaller band gap energy compared to $MoTe_2$. This indicates that $MoSe_2$ has more affinity to undergo faster electronic transition than the $MoTe_2$ upon the absorption of the particular wavelength of light. From the observation of the band structure of the considered materials, we found that the distance from the valence band maximum to the Fermi energy level is shorter than that from the conduction band minimum to the Fermi energy level. This means a greater number of band states (charge carriers) are present in the valence band than in the conduction band; hence, the materials exhibit p-type semiconducting nature. Hence, based on these findings, we conclude that both materials are p-type semiconductors, and have direct band gap energies. Thus, $MoSe_2$ and $MoTe_2$ materials are good absorbers of visible light and infrared radiation due to their small band gaps because for infrared region, photon energy range is found to be (0.001 – 1.65) eV, and for visible region, photon energy range is found to be (1.65 -3.26) eV. Therefore, they can be used in the fields of photoelectronic applications.

Density of state (DOS)

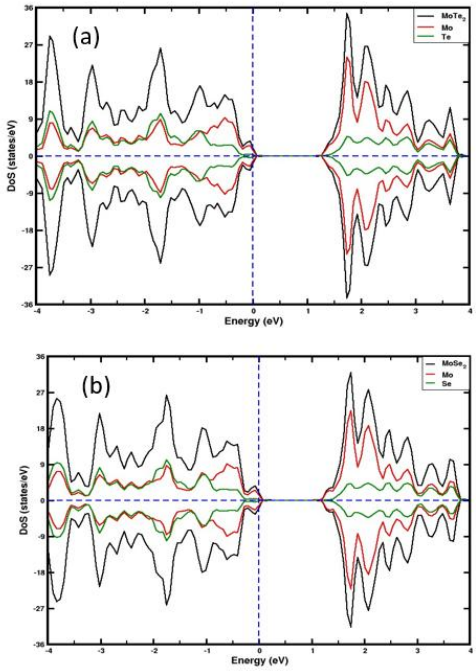

Figure 4: (Color online) (a) DoS plot of $MoTe_2$, and (b) DoS of $MoSe_2$ with Fermi level at 0 eV, where vertical dotted line separates region to the left of Fermi level is valence band and region to right is conduction band and horizontal dotted line distinguishes between up spin and down spin.]

Density of states (DoS) is defined as the number

of states per unit of energy range. DoS is used to study electronic occupational probability in the materials. High DoS implies higher occupation probability at a given energy interval, but a lack of DoS means there are no states available for occupation. Therefore, the DoS plot is essential for understanding the electronic properties of materials [33, 34]. **Figures 4(a) and 4(b)** represent DoS plots of $MoTe_2$ and $MoSe_2$ materials. In **Figure 4(a)**, the DoS plot of monolayer $MoTe_2$ is shown along with the TDoS of molybdenum and tellurium atoms. The up-and-down-spin channels are separated by a blue horizontal dotted line. As the curves suggest, the DoS at the top of the valence band (VB) (near Fermi level) is composed mainly of Mo-atoms, with a very small contribution from the Te-atom. Similarly, the bottom of the conduction band (CB) is also due to Mo atom, where the Te atom has no contribution. This suggests that the Mo atom is the dominant element in $MoTe_2$ material, which is also supported by the theoretically reported data [35]. So, it is only natural to assume that molybdenum plays a significant part in determining the electronic properties of the material. A deeper analysis (done using a PDoS plot) shows that the DoS contributions for the Mo atom are mainly composed of 4d electrons, whereas for the Te atom, the contributions come from 5p electron states. The curves in figure-4(b) illustrate the DoS plot of a $MoSe_2$ supercell structure. As can be seen from the figure, molybdenum again contributes to the top of VB and the bottom of CB, with high contributions from 4d orbital electrons. So, again, Mo atom is the dominant element, with similar characteristics to that of $MoTe_2$, and once determines various electronic properties of $MoSe_2$ as well. For the Se atom, the contributions come from 4p electron states. Here, the nature of both graphs is quite similar. This can be attributed to the Mo atom's dominance in determining the nature of both materials. From both figures, we see that the Fermi level is closer to the valence band, which supports the result obtained from the band structure analysis. There are more band states available at the Fermi level, however there is a band gap in the conduction region supporting our previous result that the materials are semiconducting in nature. There are few electronic states present at the Fermi level suggesting electrons can be excited into the conduction band more easily. Furthermore, it suggests that few electrons can be excited thermally in the conduction region which results in poor conduction at low temperatures.

Magnetic Properties

DoS plot is also used to study the magnetic properties of a material, since the magnetic properties of a material are related to density of states [36, 37]. If the DoS has symmetrically distributed spin states (i.e. up-spin and down-spin), then the material is considered to be non-magnetic. However, asymmetrical distribution of up-spin and down-spins states indicates that the material has magnetic properties. The better understand the magnetic properties of the material, we have analyzed the partial density of states (PDoS). **Figure 5(a) and 5(b)** respectively represent the PDoS plots of $MoTe_2$ and $MoSe_2$ materials. In the **Figure 5(a)**, both up-spin and down-spin states of electrons present in the individual orbital of atoms in the materials are symmetrically distributed around the Fermi energy level. This gives a net magnetic moment value of 0 μ_B/cell. This means that the $MoTe_2$ (3×3) supercell structure has non-magnetic nature. The electronic configuration of the Mo atom is [Kr] $4d^5$ $5s^1$. We analyzed the PDoS plots of Mo atom, and in both cases, we found that there is no significant contribution of spin states of electrons in the

4p orbitals of atoms, which also agrees with the theoretical prediction of the materials [38].

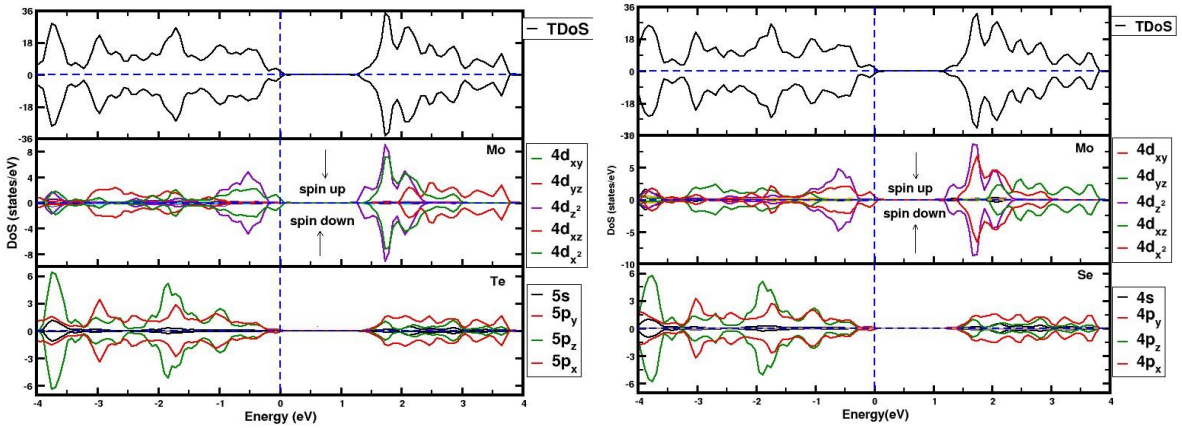

Figure 5: (Color online) (a) PDoS plot of supercell $MoTe_2$, (b) PDoS plot of supercell $MoSe_2$, where in both plots, vertical dotted lines represent Fermi energy, which separates the valence and conduction bands.

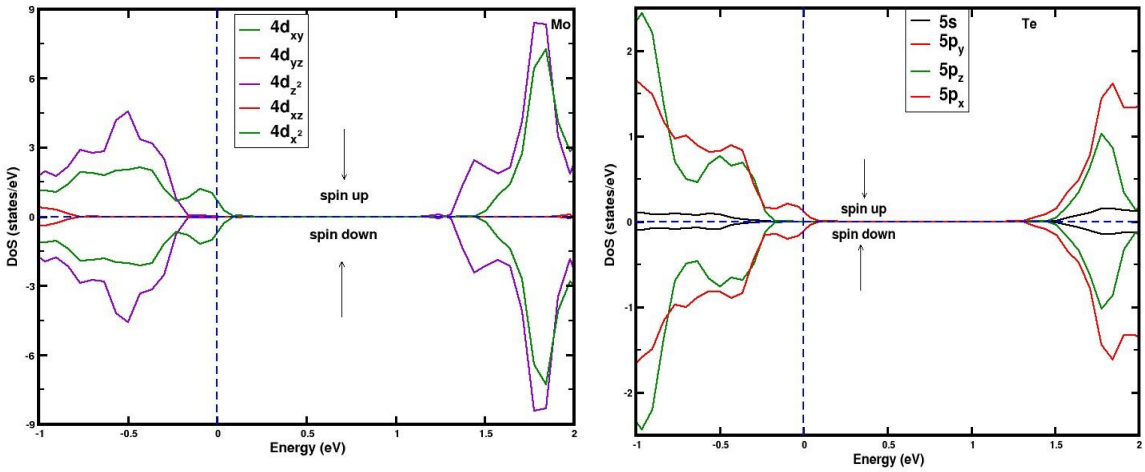

Figure 6: (Color online) (a) PDoS plot of Mo- atom in $MoTe_2$, (b) PDoS plot of Te-atom in $MoTe_2$, where in both plots vertical dotted lines represents Fermi energy, which separates the valence and conduction bands.

Similarly, the 5s orbital has very little contribution to the production of the magnetic moment. So, most of the contribution to the PDoS comes from the 4d orbital. Further analysis performed to study the contribution from sub-orbitals shows hybridization between $4d_{xy}$ and $4d_x2$, and hence they have equal contribution to the DoS of the Mo atom. Moreover, there is another overlap in the sub-orbitals $4d_{yz}$ and $4d_{xz}$ as well. The graph reveals that the DoS at the Fermi level is due to the $4d_{xy}$ and $4d_x2$ orbitals of the Mo atom. The total magnetic moment produced by the 5s, 4p and 4d-orbitals of electrons is the same and equals 0 μ_B/cell. Similarly, the electronic configuration of the Te atom is [Kr] $4d^{10}$ $5s^2$ $5p^4$. When the PDoS plot for the Te atom is analyzed, we saw that the highest contribution comes from 5p orbital, as there is no contribution from the 4d orbital and very little contribution from the 5s orbital in the structure. Moreover, the sub-orbitals $5p_y$ and $5p_x$ overlap with each

other and have DoS at the Fermi level as well. The total magnetic moments produced by the spin states of electrons in the 5s, 4p, and 4d orbitals of the atoms have the same value, which is equal to 0 μ_B/cell. This shows that the up and down spin states in the orbitals as well as sub-orbitals are symmetrically distributed in the case of monolayer $MoTe_2$ material. The PDoS of plots of Mo, and Te atoms in $MoTe_2$ material are illustrated in figures-6(a) and 6(b) respectively.

The **Figure 5(b)** illustrates the the PDoS plot of $MoSe_2$ material. Similar to $MoTe_2$, $MoSe_2$ also has non-magnetic properties. The PDoS of molybdenum in $MoSe_2$ is similar to that of the $MoTe_2$ material. As we know, the electronic configuration of $MoSe_2$ is [Ar] $3d^{10},4s^2$, $4p^4$. As can been from figure-5(b), the contribution to the PDoS by up-spin and down-spin states comes only from the 4p-orbitals. The contribution at the Fermi level for the Se atom comes from the $4p_y$ and $4p_x$ orbitals. As is the case with tellurium, the $4p_y$ and $4p_x$ sub-orbitals overlap with each other for the selenium atom. All the spin channels of different orbitals are symmetrically distributed for the Se atom as well, implying the non-magnetic behaviors of the Se atom and $MoSe_2$ material as a whole. More clearly, we have developed a PDoS plot for Se atoms in $MoSe_2$, which is shown in **Figure 7**. The estimated values of magnetic moment given by the distributed up-and down-spin states elections in the individual orbitals of Mo, Te, & Se atoms in the $MoTe_2$ and $MoSe_2$ materials are given in **Table 3.**

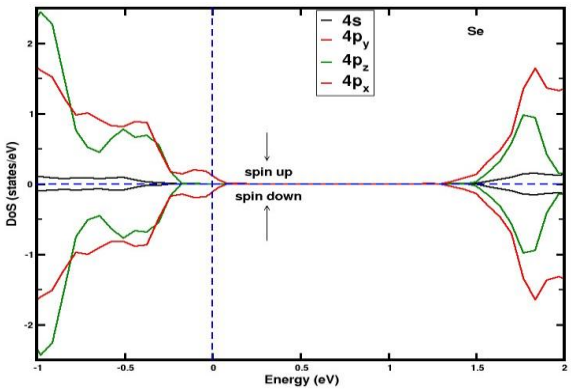

Figure 7: (Color online): PDoS plot of Se-atom in $MoSe_2$, where vertical dotted line represents Fermi energy level, which separates the valence and conduction bands.]

Dynamical Properties

Dynamical properties of considered materials are studied by the analysis of their phonon dispersion curve, which is given as following

Phonon Dispersion

Dynamic stability is an important property of a material, as it helps in classifying the material as unstable, metastable, or stable [39, 40]. If a material is mechanically and dynamically stable, then the material is considered to be structurally stable. This has profound implications for its application in the electronics field. To study the dynamic stability of the material, we have used a phonon dispersion curve. The figures-8(a) and 8(b) show the phonon dispersion relation between highly symmetric points (Γ, M, K, Γ, A, L, H) and the frequency of phonon waves. Two types of frequency branches (acoustic branch and optical branch) are seen in the **Figures 8(a)** and **8(b)**. The acoustic branch is the lower frequency branch, where two particles in a unit cell oscillate in phase. In contrast, particles in the optical branch have a higher frequency, (hence, higher energy) and the particles oscillate in opposite directions (move out of phase with each other). In our phonon curves, there are three acoustic waves and six optical

waves. The frequencies of both acoustic and optical branches are estimated at the high symmetric points. The phonon (optical) band gap energy of $MoTe_2$ and of $MoSe_2$ materials are estimated and given in **Table 4**. Here, we have calculated the maximum acoustic frequency and minimum optical frequency at symmetric points to determine the phonon band gap energy of the considered materials.

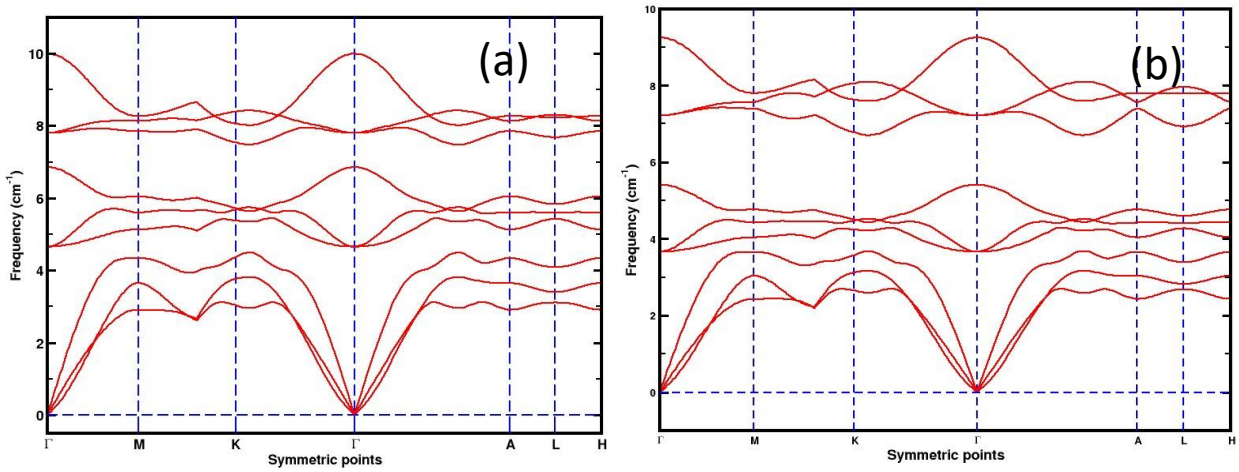

Figure 8: (Color online): (a) phonon dispersion curve of $MoTe_2$ supercell structure, and (b) phonon dispersion curve of $MoSe_2$ supercell structure, where vertical dotted lines represent highly symmetric points, and vertical dotted line represents zero frequency point. The frequency is in the unit cm^{-1}.

Table 3: The magnetic moments given by up-and down-spin states of electrons in the individual orbitals of Mo, Se and Te atoms in $MoTe_2$ and $MoSe_2$ materials using PBE+U functional**.**

Orbitals	$MoTe_2$ (μ_B/*cell*)				$MoSe_2$ (μ_B/*cell*)			
	Mo		Te		Mo		Se	
	Up-spin	Down-spin	Up-spin	Down-spin	Up-spin	Down-spin	Up-spin	Down-Spin
s	0.09	-0.09	0.69	-0.69	0.09	-0.09	0.68	-0.68
p_y	0.04	-0.04	0.47	-0.47	0.03	-0.03	0.44	-0.44
p_z	0.04	-0.04	0.42	-0.42	0.04	-0.04	0.41	-0.41
p_x	0.03	-0.03	0.47	-0.47	0.04	-0.04	0.44	-0.44
d_{xy}	0.39	-0.39	0.01	-0.01	0.38	-0.38	0.01	-0.01
d_{yz}	0.35	-0.35	0.01	-0.01	0.34	-0.34	0.01	-0.01
d_z^2	0.38	-0.38	0.007	-0.007	0.38	-0.38	0.007	-0.007

d_{xz}	0.35	-0.35	0.01	-0.01	0.34	-0.34	0.01	-0.01
d_{x}^2	0.39	-0.39	0.01	-0.01	0.38	-0.38	0.01	-0.01

It is clear that optical phonons have higher oscillation frequencies than acoustic phonons. Moreover, acoustic phonons have zero frequency at symmetric points (Γ). This is a strong indication that our materials are dynamically stable. Furthermore, neither acoustic phonons nor optical phonons have imaginary frequencies throughout the Brillouin zone (BZ). Due to the positive frequency of phonons, it is concluded that monolayer $MoTe_2$ and $MoSe_2$ are dynamically stable materials. Hence, these materials can be used to create reliable, flexible, and high-performance devices.

Table 4: Phonon band gap energy (PBG) of $MoTe_2$ and $MoSe_2$ materials are estimated using the values of acoustic maximum frequency (AMF) and optical minimum frequency (OMF) at high symmetric points. All the values have been calculated using phonon dispersion curves. The values of frequencies are given in cm^{-1}.

Highly	AMF (cm^{-1})		OMF (cm^{-1})		PBG (cm^{-1})	
Symmetric Points	$MoTe_2$	$MoSe_2$	$MoTe_2$	$MoSe_2$	$MoTe_2$	$MoSe_2$
Γ	0	0	3.68	4.65	3.68	4.65
M	3.63	4.33	4.01	5.11	0.38	0.78
K	3.57	4.35	4.23	5.35	0.66	1.00
Γ	0	0	3.65	4.64	3.65	4.64
A	3.63	4.34	4.02	5.11	0.39	0.77
L	3.38	4.08	4.23	5.42	0.85	1.34
H	3.66	4.33	4.06	5.12	0.40	0.79

Conclusion

In the present work, we investigated the structural, electronic, magnetic, and dynamical properties of $MoTe_2$ and $MoSe_2$ (3×3) supercell structures. All the calculations performed using the density functional theory (DFT) approach with the computational tool quantum ESPRESSO. Firstly, we studied structural properties of the considered materials using ground state energy and the bond length of atoms present in the structures. The structural analysis reveals that both TMDCs materials are structurally stable and have a hexagonal form. $MoSe_2$ and $MoTe_2$ have equal minimum ground state energies of -244.20 eV, which means that the materials are structurally stable. The electronic properties of $MoTe_2$ and $MoSe_2$ materials are investigated by analyzing the band structure and density of states (DoS) plots. From the calculations of the band structure and DoS plots, it is found that both considered materials are p-type semiconductors. The band gap energy of $MoSe_2$ is found to be 1.31 eV, which is smaller as compared to the band gap energy of $MoTe_2$ (1.40 eV). This suggests that $MoSe_2$ can be used for effective absorption of visible and infrared radiation. To explore the magnetic properties of materials, the material's density of states (DoS) and partial density of states (PDoS) were analyzed. In both plots, we analyzed the distribution of up-spin and down-spin states of electrons in the individual atoms present in the material. That are found to be symmetrically distributed, hence net magnetic moment of the material is found to be zero. Thus, $MoTe_2$ and $MoSe_2$ have non-magnetic properties. Moreover, we have developed the phonon distribution curves of the phonon waves of the studied materials. It is found that the phonon dispersion frequencies at all symmetric points have positive values. This conclusively proves that both materials are dynamically stable. Therefore, from the analysis of the materials electronic, magnetic, dynamical properties, it is found that $MoTe_2$ and $MoSe_2$ are semiconducting, non-magnetic, and dynamically stable materials. Based on these determined properties, we recommend

that $MoTe_2$ and $MoSe_2$ can be used in the fields o.

Acknowledgements

The authors would like to acknowledge the Condensed Matter Research Lab CDP TU, TWAS Research Funds RG 20-316, Network Project NT-14 of ICTP/OE for the computing capacity, and Prof. NP Adhikari for his excellent input on the manuscript.

Author's Contribution Statement

A. Pokharel: Generated the data, Writing: original draft, **K. Khanal:** Formal analysis, Writing: original draft, **S. K. Yadav:** Formal data analysis, Writing: review &editing **T. Neupane:** Writing: review & editing, **G. Paudel:** Writing: review &editing**, O. S. Rijal:** Writing: review &editing, **H. K. Neupane**: Conceptualization, Data curation, Investigation, Methodology, Supervision, Visualization, Writing: review & editing**.**

Conflict of Interest

The authors attest that no known financial or personal conflicts of interest may have influenced any of the work included in this paper.

Data Availability Statement

The corresponding author can provide the data used to construct figures and tables upon request.

References

1. A. K. Mia, M. Meyyappan, and P. K. Giri, Two-dimensional transition metal dichalcogenide based biosensors: from fundamentals to healthcare applications, *Biosensors*, 2023, 13 (2), 169. https://doi.org/10.3390/bios13020169.
2. K. S. Novoselov, D. Jiang, F. Schedin, T. J. Booth, V. V. Khotkevich, S. V. Morozov A. Geim, Two-dimensional atomic crystals, *Proceedings of the National Academy of Sciences*, 2005, 102 (30), 10451-10453. https://doi.org/10.1073/pnas.0502848102.
3. F. Sabry, Graphene: The key to clean, and unlimited energy, so the next generation of smart devices could be powered by nano-scale power generators, *One Billion Knowledgeable,* 2022, 8.
4. Z. Zhen, and H. Zhu. "Structure and properties of graphene, *Graphene*. Academic Press, 2018, 1-12. https://doi.org/10.1016/B978-0-12-812651-6.00001-X.
5. M. D'angelo, and I. Matsuda, Basics and families of monatomic layers: Single-layer 2D materials, *Monatomic Two-Dimensional Layers*. Elsevier, 2019, 3-22. https://doi.org/10.1016/B978-0-12-814160-1.00001-0.
6. M. Pumera, Z. Sofer, and A. Ambrosi, Layered transition metal dichalcogenides for electrochemical energy generation and storage, *Journal of Materials Chemistry A*, 2014, 2 (24) 8981-8987. https://doi.org/10.1039/C4TA00652F.
7. D. Puotinen, and R. E. Newnham, The crystal structure of MoTe2, *Acta Crystallographica*, 1961, 14(6) 691-692. https://doi.org/10.1107/S0365110X61002084
8. B. E. Brown, The crystal structures of WTe2 and high-temperature $MoTe_2$, *Acta Crystallographica* 20 (2), 268-274. https://doi.org/10.1107/S0365110X66000513.
9. K. Balakrishnan, and P. Ramasamy. Study of anomalous electrical behaviour of molybdenum ditelluride single crystals, *Journal of crystal growth*, 1994, 309-311. https://doi.org/10.1016/0022-0248(94)91291-2.
10. C. Ruppert, O. B. Aslan, and T. F. Heinz, Optical properties and band gap of single-and few-layer $MoTe_2$ crystals, *Nano Letters*, 2014, 6231-6236. https://doi.org/10.1021/nl502557g.
11. L. Zhang, and A. Zunger, Evolution of electronic structure as a function of layer thickness in group-VIB transition metal dichalcogenides: emergence of localization prototypes, *Nano Letters*, 2015, 15(2), 949-957. https://doi.org/10.1021/nl503717p.

12. B. M. Kanoun, Tuning magnetic properties of two-dimensional $MoTe_2$ monolayer by doping 3d transition metals: Insights from first principles calculations, *Journal of Alloys and Compounds*, 2018, 748, 938-942. https://doi.org/10.1016/j.jallcom.2018.03.132.
13. P. Johari, and V. B. Shenoy, Tuning the electronic properties of semiconducting transition metal dichalcogenides by applying mechanical strains, *ACS Nano*, 2012, 6(6) 5449-5456. https://doi.org/10.1021/nn301320r.
14. T. J. Wieting, A. Grisel, and F. Levy, Interlayer bonding and localized charge in $MoSe_2$ and α-$MoTe_2$, *Physica B+ C*, 1980, 99 (4), 337-342. https://doi.org/10.1016/0378-4363(80)90256-9.
15. M. Tebyetekerwa, J. Zhang, Z. Xu, T.N. Truong, Z.L. Yin, … and H.T. Nguyen, Mechanisms and applications of steady-state photoluminescence spectroscopy in two-dimensional transition-metal dichalcogenides, *ACS Nano*, 2020, 14 (11),14579-14604. https://doi.org/10.1021/acsnano.0c08668.
16. B. Mortazavi, G.R. Berdiyorov, M. Makaremi, and T. Rabczuk, Mechanical responses of two-dimensional MoTe2; pristine 2H, 1T and 1T′ and 1T′/2H heterostructure, *Extreme Mechanics Letters*, 2018, 20, 65-72. https://doi.org/10.1016/j.eml.2018.01.005.
17. H. K. Neupane, and N. P. Adhikari, First-principles study of structure, electronic, and magnetic properties of C sites vacancy defects in water adsorbed graphene/MoS2 van der Waals heterostructures, *Journal of Molecular Modeling*, 2021, 27(3), 82. https://doi.org/10.1007/s00894-021-04690-8.
18. H. K. Neupane, and N. P. Adhikari, Tuning Structural, Electronic, and Magnetic Properties of C Sites Vacancy Defects in Graphene/MoS2 van der Waals Heterostructure Materials: A First-Principles Study, *Advances in Condensed Matter Physics,* 2020, 2020 (1), 8850701. https://doi.org/10.1155/2020/8850701.
19. H. K. Neupane, and N. P. Adhikari, Effect of vacancy defects in 2D vdW graphene/h-BN heterostructure: First-principles study, *AIP Advances*, 2021, 11(8), 085218. https://doi.org/10.1063/5.0059814.
20. L. J. Bartolotti, and K. Flurchick, An introduction to density functional theory, *Reviews in computational chemistry*, 1996, 187-216. (DOI: 10.1002/9780470125847.
21. M. Orio, D. A. Pantazis, and F. Neese, Density functional theory, *Photosynthesis Research*, 2009, 102, 443-453. https://doi.org/10.1007/s11120-009-9404-8.
22. W. Kohn, and L. J. Sham, Self-consistent equations including exchange and correlation effects, *Physical Review*, 1965, 140(4A), A1133. https://doi.org/10.1103/PhysRev.140.A1133.
23. A. Dal Corso, A pseudopotential plane waves program (pwscf) and some case studies, *Quantum-mechanical Ab-initio calculation of the properties of crystalline materials*, 1996, 155-178. https://doi.org/10.1007/978-3-642-61478-1-10.
24. F. Giustino, *Materials modelling using density functional theory: properties and predictions*. Oxford University Press, 2014.ISBN: 978-0-19-966243-2.
25. T. Van Voorhis, and G. E. Scuseria, A novel form for the exchange-correlation energy functional, *The Journal of Chemical Physics*, 1998, 109 (2), 400-410. https://doi.org/10.1063/1.476577.
26. D. J. Griffiths, and D. F. Schroeter. *Introduction to quantum mechanics*. Cambridge university press, 2018. https://ui.adsabs.harvard.edu/abs/2016iqm..bookG.
27. A. Kokalj, Computer graphics and graphical user interfaces as tools in simulations of matter at the atomic scale, *Computational Materials Science*, 2003, 28 (2), 155-168. https://doi.org/10.1016/S0927-0256(03)00104-6.
28. Y. Wang, P. Wisesa, A. Balasubramanian, S. Dwaraknath, and T. Mueller, Rapid generation

of optimal generalized Monkhorst-Pack grids, *Computational Materials Science*, 2021, 187, 110100. https://doi.org/10.1016/j.commatsci.2020.110100.

29. O. Knop, and R. D. MacDonald, Chalkogenides of the transition elements: III. Molybdenum ditelluride." *Canadian Journal of Chemistry*, 1961, 39(4), 897-904. https://doi.org/10.1139/v61-11.
30. F. Romanens, S. Pizzini, J. Sort, F. Garcia, J. Camarero, ...and B. Dieny, Magnetic relaxation measurements of exchange biased (Pt/Co) multilayers with perpendicular anisotropy." *The European Physical Journal B-Condensed Matter and Complex Systems*, 2005, 45, 185-190. DOI: 10.1140/epjb/e2005-00053-3.
31. Y. Ma, Y. Dai, M. Guo, C. Niu, J. Lua, and B. Huanga, Electronic and magnetic properties of perfect, vacancy-doped, and nonmetal adsorbed $MoSe_2$, $MoTe_2$ and WS_2 monolayers, *Physical Chemistry Chemical Physics*, 2011, 13(34), 15546-15553. https://doi.org/10.1039/C1CP21166H.
32. S. Tongay, J. Zhou, C. Ataca, K. Lo, T. S. Matthews, .. J. Wu, Thermally driven crossover from indirect toward direct bandgap in 2D semiconductors: $MoSe_2$ versus MoS_2, *Nano Letters,* 2012, 12(11),5576-5580. https://doi.org/10.1021/nl302584w.
33. M. Nepal, G. Paudel, S. Aryal, A. Devkota, and H. K. Neupane, Adsorption of water on vacancy defective h-bn bilayer at b and n sites: First-principles calculation, *BIBECHANA*, 2024, 21(2), 129-141. https://doi.org/10.3126/bibechana.v21i2.62607.

34. S. Aryal, G. Paudel, M. Nepal, D. Oli, O.S. Rijal, and H. K. Neupane, Water Adsorption on Pristine and Vacancy Defected h-BN Monolayer: First-principles Stud, *Journal of Institute of Science and Technology*, 2025, 30(1), 73-81. https://doi.org/10.3126/bibechana.v21i2.62607.

35. M. G. Menezes, and S. Ullah, Unveiling the multilevel structure of mid gap states in Sb-doped MoX_2 (X= S, Se, Te) monolayers, *Physical Review B,* 2021, 104 (12), 125438. https://doi.org/10.1103/PhysRevB.104.125438.
36. G. Paudel, M. Nepal, S. Aryal, A. Devkota, and H. K. Neupane, Effect of water adsorption on bilayer h-BN: First-principles study, *Journal of Nepal Physical Society*, 2023, 9(2), 56-62. https://doi.org/10.3126/jnphyssoc.v9i2.62323.
37. H. K. Neupane, and N. P. Adhikari, Adsorption of water on C sites vacancy defected graphene/h-BN: First-principles study, *Journal of Molecular Modeling*, 2022, 28(4), 107. https://doi.org/10.1007/s00894-022-05101-2.
38. J. R. Mohanty, Effect of Nm (B, C, N, O and F) Doping and Fe-Nm Co-Doping Onstructure, Electronic and Magnetic Properties of Monolayer2h-$MoTe_2$: A First Principles Investigation. Physica E: Low-dimensional Systems and Nanostructures, 2024, 156, 115846. https://doi.org/10.1016/j.physe.2023.115846.
39. M. W. Qureshi, X. Ma, G. Tang, and R. Paudel, Structural stability, electronic, mechanical, phonon, and thermodynamic properties of the M_2GaC (M= Zr, Hf) max phase: an AB initio calculation, *Materials,* 2020, 13(22), 5148. https://doi.org/10.3390/ma13225148.
40. O. S. Rijal, H. K. Neupane, D. Oli, R. K. Neupane, P. Shrestha, S. Sharma, ... & R. Parajuli, A first-principles investigation of the structural, mechanical, dynamic, electronic, magnetic, and optical properties of Ti_2AC (A= Cd, S) MAX phase compounds." *Journal of Physics D: Applied Physics*, 2025, 58(12), 125102. DOI 10.1088/1361-6463/ada808.